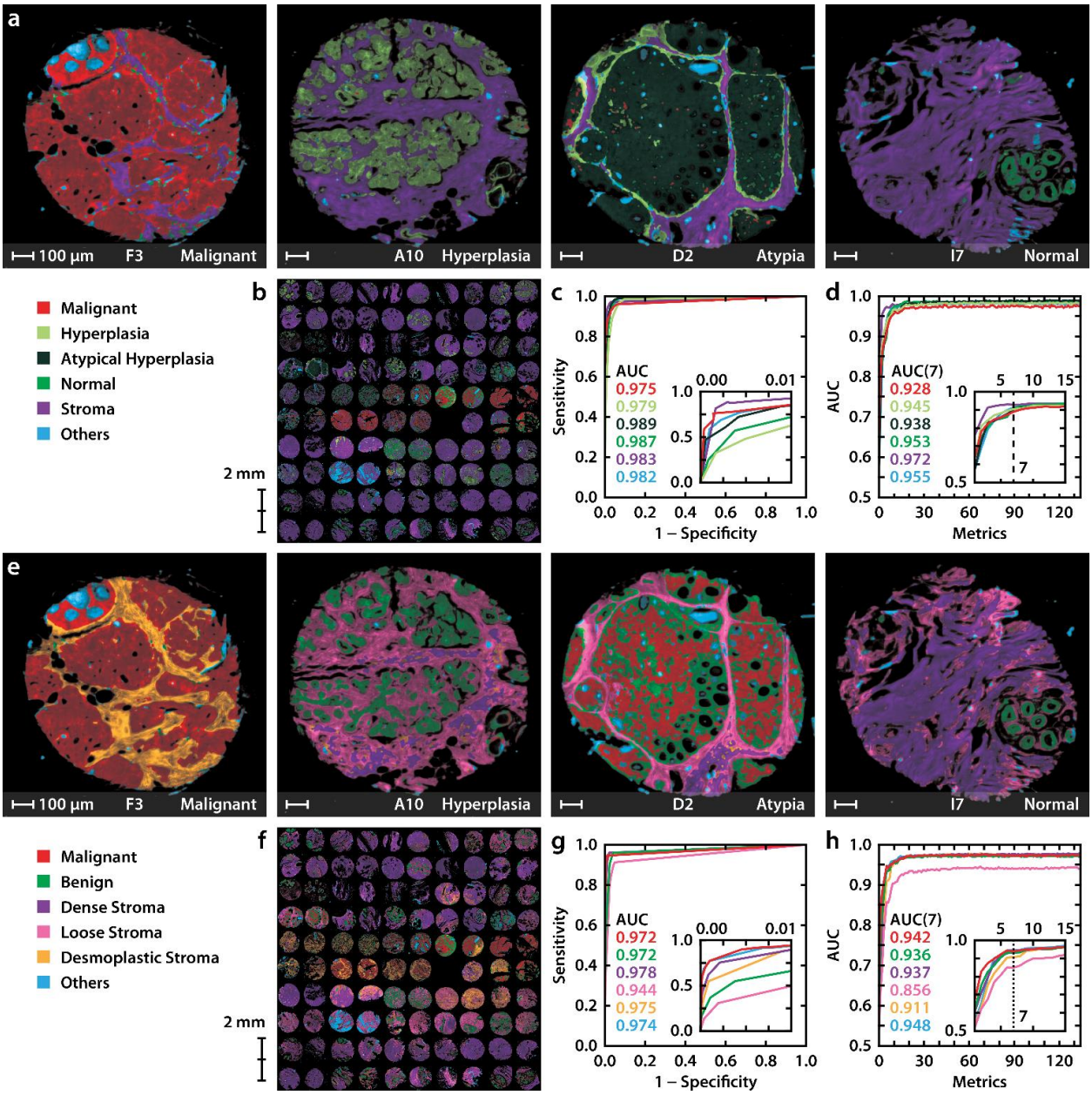


**Fig. 1. Epithelial tumor classification and microenvironment models for breast cancer characterization using FT-IR imaging.** Using the 6-class epithelial (6E) model, (**a**) classified images showing malignant, hyperplasia, atypia, and normal tissue samples, **(b)** 6E class image of the full tissue microarray (TMA), **(c)** the corresponding receiver operating characteristic (ROC) curve, and **(d)** Area under the curve (AUC) of the ROC curve dependence on spectral metrics for the 6E model. The inset shows that the accuracy saturates for a few metrics. The complementary 6-class stromal (6S) model on the same samples shows **(e)** disease associated microenvironment changes, **(f)** 6S classification of the TMA, **(g)** the corresponding ROC curve, and **(h)** the impact spectral metrics on AUC values for the 6S model.

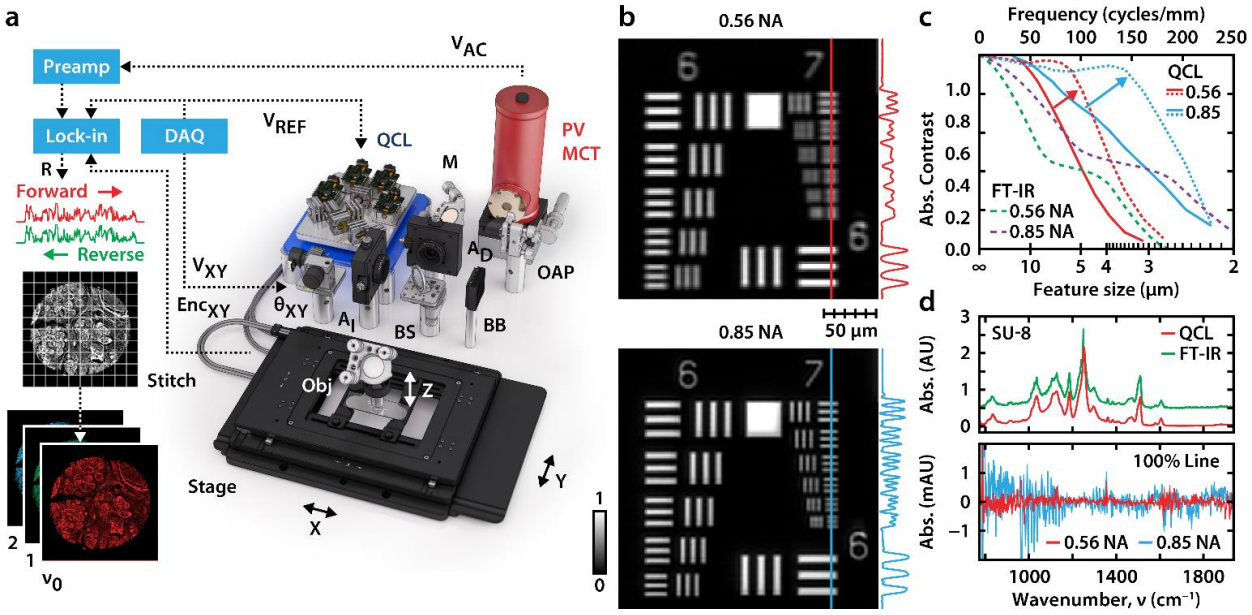


**Fig. 2. Laser-based confocal infrared microscopy.** (**a**) The microscope consists of a quantum cascade laser (QCL) source, tunable for narrow-band emission across the mid-IR fingerprint region. A high-speed stage and focus unit raster scans the sample, while the detection is locked into the laser's pulse rate and each pixel is triggered by the stage encoder counter. (**b**) Images of USAF 1951 resolution test targets show diffraction limited performance for absorbance at 1658 $cm^{-1}$ with both the 0.56 NA objective (top) at 2 µm pixel size and the 0.85 NA objective (bottom) at 1 µm pixel size. (**c**) The optical contrast of each set of bars is plotted as a function of spatial frequency. The bars are no longer resolvable if the contrast drops below 26%, which corresponds to the Rayleigh criterion separation distance. The arrow indicates the deconvolution of the raw data (solid line) with the simulated PSF at the specified wavenumber to achieve a substantial resolution enhancement (dotted line). These results are compared to the simulated performance (dashed line) of a FT-IR instrument with optimized Schwarzschild objectives used in FT-IR imaging. (**d**) The unprocessed spectrum of a 5 µm layer of SU-8 epoxy acquired by our QCL instrument at 1 $cm^{-1}$ resolution shows accurate spectral features compared to a reference FT-IR spectrometer. The 100% spectral profile lines show absorbance noise of ~$10^{-4}$ and $10^{-3}$ for the two objectives over most the fingerprint region.

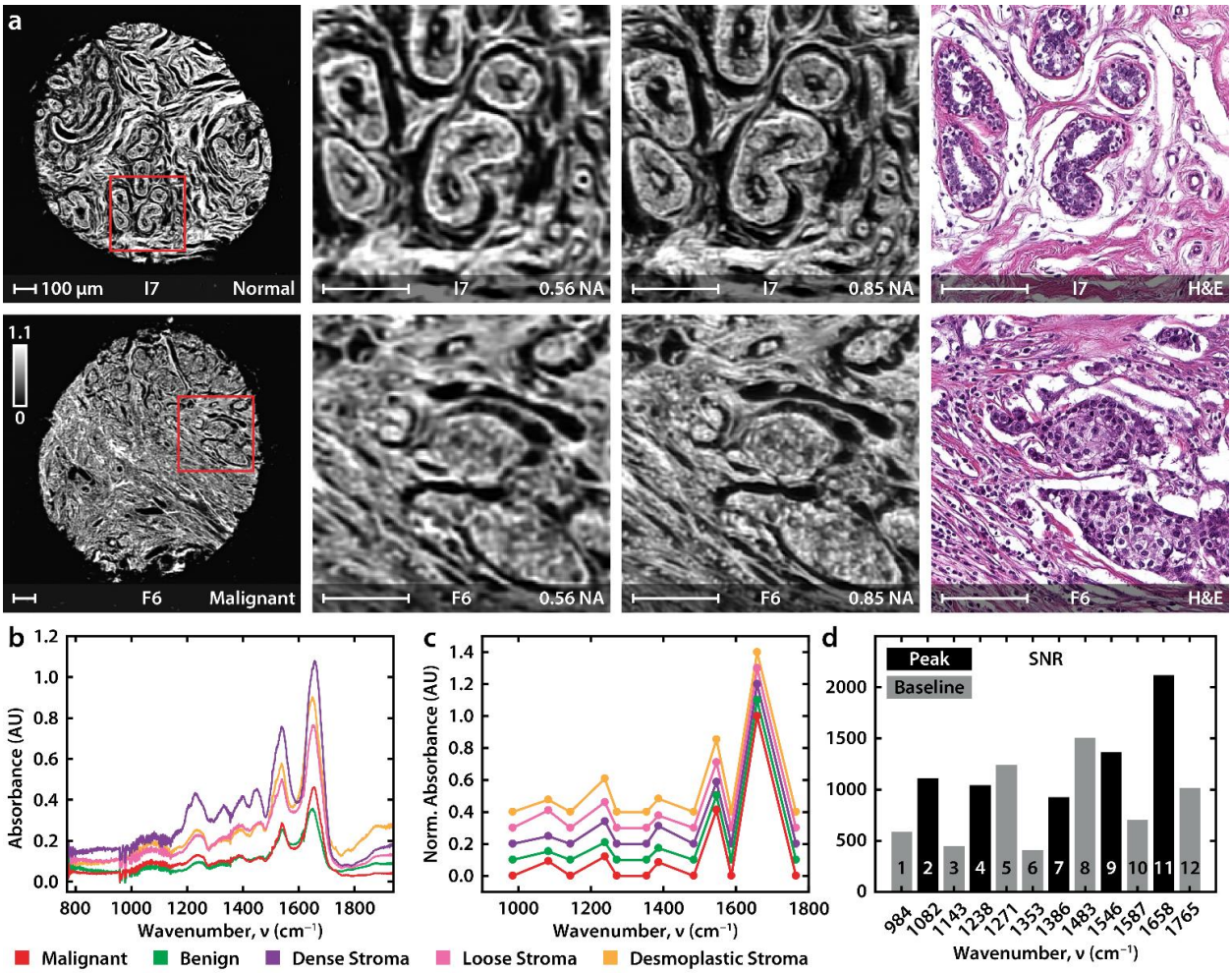


**Fig. 3. High-definition imaging of breast tissue.** (**a**) A selection of one normal and one malignant tissue sample from a 20 x 20 mm TMA, acquired at 0.56 NA and 0.85 NA at 2 µm and 1 µm per pixel, respectively. The absorbance at 1658 $cm^{-1}$, indicative of the Amide I vibrational mode, is shown in the image and enlarged subsections that are compared to an H&E stained image of a serial section. (**b**) Point spectra from five tissue types at 1 $cm^{-1}$ resolution; spectra are offset for clarity. (**c**) Normalized and baselined point spectra from five tissue types at discrete frequencies. **(d)** Average SNR for important spectral features.

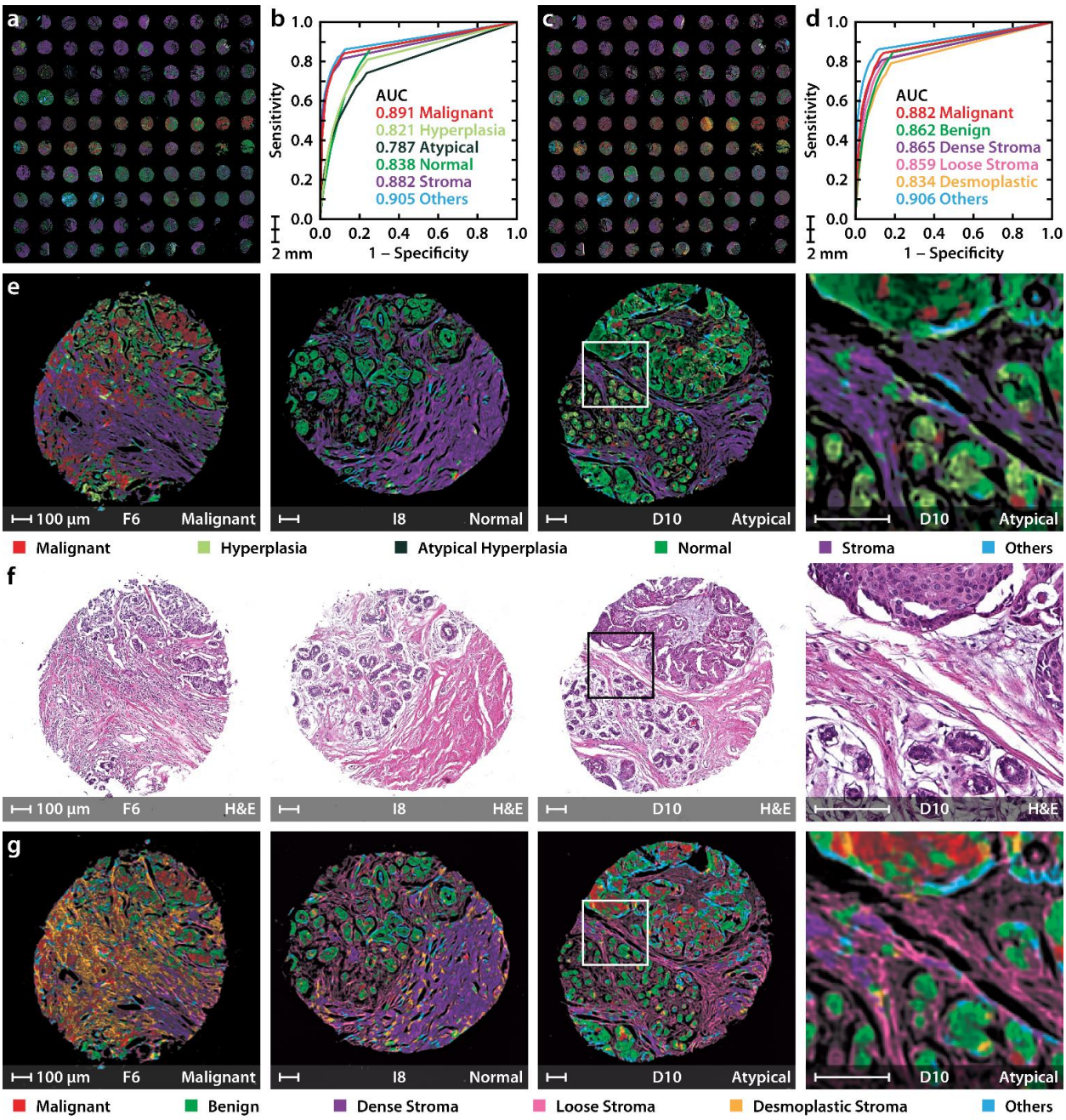


**Fig. 4. Discrete frequency epithelial and stromal classification for rapid breast cancer diagnosis.** (**a**) TMA classified using the 6-class epithelial (6E) model. **(b)** Receiver operating characteristic (ROC) curves represent the performance of each class in the 6E model. **(c)** TMA classified using the 6-class stromal (6S) differentiation model. **(d)** ROC curves for the 6S model. **(e)** 6E model classified images of three samples from the TMA with malignant, normal and atypical hyperplasia states (left to right) along with their corresponding H&E stained images in **(f)**. **(g)** Classification using the 6S model. A small region from the hyperplasia with atypia sample is also shown, along with its H&E stain, to demonstrate the spatial distribution of normal and malignant cells. The letter and numbers below each image correspond to the row and column of the TMA (A1 is the top left sample), respectively. All scale bars shown here are 100 µm

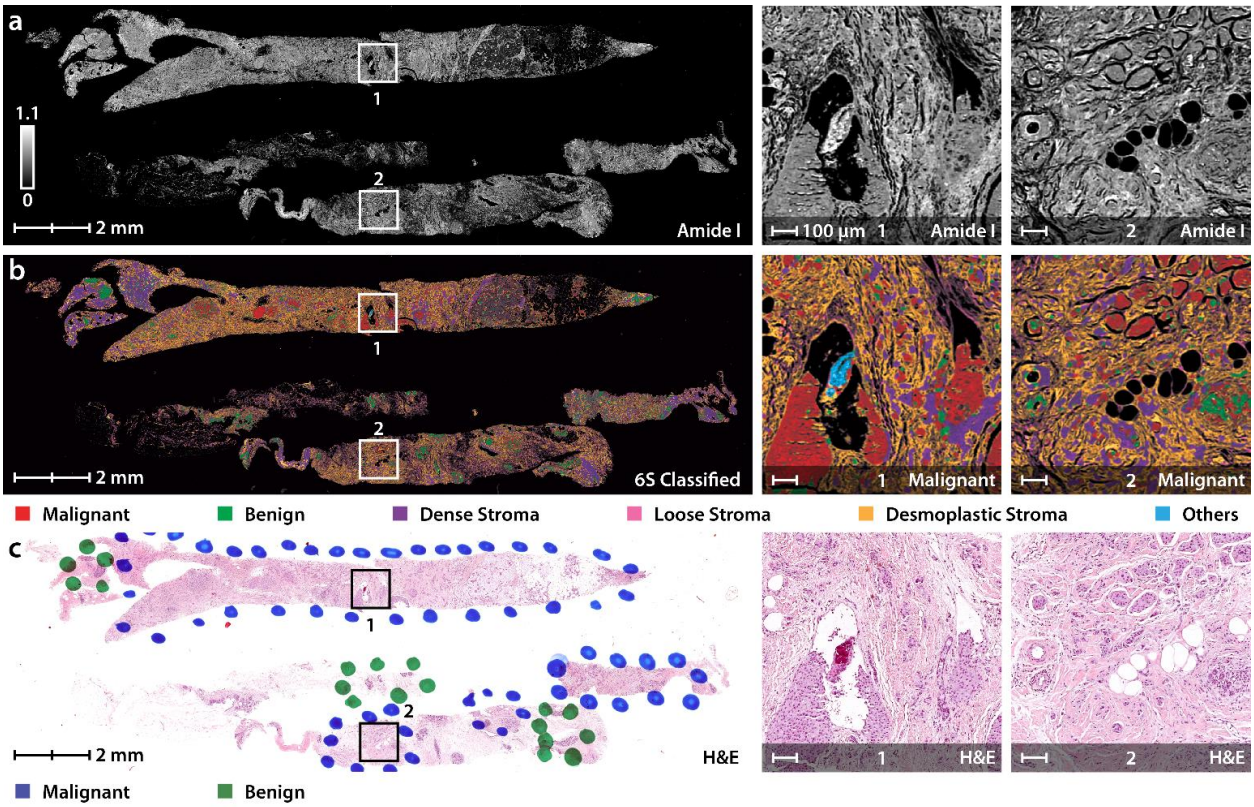


**Fig. 5. Rapid triaging of malignant sections using stainless imaging of human breast biopsy samples in feasible times. (a)** Image of needle biopsy sections using absorbance at 1658 $cm^{-1}$ with specific malignant regions enlarged for clarity. **(b)** The multispectral image was classified using a six class model separating cancerous and normal epithelial cells from various collagen-rich stromal types (6S). **(c)** Pathologist annotations to the H&E stained image of a consecutive section demonstrate agreement with the IR classified image.